Melting studies of indium: determination of the structure and density of melts at high pressures and high temperatures

2002 J. Phys.: Condens. Matter 14 10533

(http://iopscience.iop.org/0953-8984/14/44/328)

INSTITUTE OF PHYSICS PUBLISHING JOURNAL OF PHYSICS: CONDENSED MATTER

J. Phys.: Condens. Matter **14** (2002) 10533–10540 PII: S0953-8984(02)38598-9

Melting studies of indium: determination of the structure and density of melts at high pressures and high temperatures

Guoyin Shen[1], Nagayoshi Sata[1,2], Nicolas Taberlet[3], Matthew Newville[1], Mark L Rivers[1,4] and Stephen R Sutton[1,4]

[1] Consortium for Advanced Radiation Sources, University of Chicago, Chicago, IL 60637, USA
[2] Department of Earth and Planetary Science, University of Tokyo, Bunkyo-ku, Tokyo 113-0033, Japan
[3] Department des Sciences de la Matiere, Ecole Normale Superieure, 69364 LYON Cedex 07, France
[4] Department of the Geophysical Sciences, University of Chicago, Chicago, IL 60637, USA

E-mail: shen@cars.uchicago.edu

Received 24 June 2002
Published 25 October 2002
Online at stacks.iop.org/JPhysCM/14/10533

Abstract

The melting behaviour, structure, and density of molten indium at high pressures have been studied in an externally heated diamond anvil cell (DAC) using x-ray diffraction/scattering measurements. Melting at high pressure was identified by the appearance of diffuse scattering from the melt. Analysis of the diffuse scattering shows that at 710(3) K the coordination number at the nearest neighbour increases from 10.1(4) at 1.0 GPa to 12.1(5) at 6.3 GPa. A method for measuring the density of amorphous materials is introduced for DAC studies and the first result on molten indium is presented.

(Some figures in this article are in colour only in the electronic version)

1. Introduction

As a first-order phase transition, melting exhibits discontinuities in the first derivatives of the free energy: volume and entropy. It also involves abrupt changes in electrical and thermal conductivities, magnetic susceptibility, refractive index, and other physical properties. The changes of these physical properties are often used for identification of melting at high pressures [1, 2]. Specifically, the characteristics of melting are the loss of crystalline long-range order and resistance to shear. To conclusively identify melting as distinct from other first-order phase transitions, we need knowledge of the structures or shear strength of the phases involved. Recently, with synchrotron radiation, the onset of melting of indium at high pressure was identified by the appearance of diffuse scattering with the simultaneous loss of

crystalline diffraction signals [3]. These results demonstrate the successful use of x-ray diffuse scattering as a melting criterion in the diamond anvil cell (DAC).

The observation of the diffuse scattering in a DAC offers possibilities of structure studies of melts at high pressures and high temperatures. Since the first study on liquid at high pressure more than a decade ago [4], there have been a growing number of studies on the structure of melts under high pressure, particularly with the use of synchrotron radiation [5–8]. These studies are limited to applications of large-volume presses and therefore cover limited pressure ranges. In this study, we demonstrate the feasibility of determining the structures of melts in a DAC.

The liquid–liquid (LL) phase transition for a pure substance is a subject of many studies [9–11]. Density is generally believed to be an appropriate order parameter for describing LL phase transitions [9]. Knowledge of densities of melts, fluids, and glasses (amorphous solids) is important in condensed matter physics and is a key to understanding geochemical evolution of planetary interiors. While the density of crystalline phases can be determined by x-ray diffraction to ultrahigh pressures, density measurements on melts and amorphous materials at high pressures are limited to a few systems [12, 13] using large-volume presses. Here we introduce a method for measuring the density of amorphous materials in a DAC and report the first results on molten indium. Indium was chosen for the first experiment because of its relatively low melting temperature and low reactivity.

2. Experiment

An externally heated DAC (DXR-7, Diacell) was used in this study. The main feature of the DAC design is the use of four cartridge heaters inserted in the cell body, providing heat to the entire cell and resulting in a uniform temperature distribution inside the cell. Temperatures were measured by a type-K thermocouple at the gap position between the gasket and the diamond anvil. Prior to the experiment, a second thermocouple was placed at the sample position. The cell was heated to 700 K and temperatures were measured at various power levels. The temperature at the sample position was found to be 4.5 K less than that at the gap position with a standard deviation of 1.9 K. A rhenium gasket was pre-indented to about 50 μm in thickness with diamond anvils 500 μm in culet diameter. Two holes 100 μm in diameter were drilled at the positions equidistant from the centre. Indium powder (99.999%, Alfa Aesar) was loaded into one of the holes; the other hole was loaded with NaCl. A NaCl chip ($\sim$5 μm in dimensions) was put at the corner of the chamber with indium for the pressure measurement.

The x-ray diffraction experiment was performed at GeoSoilEnviroCARS, beamline 13-ID-D, at the Advanced Photon Source (APS). A CCD detector (MAR-CCD) was used to collect diffraction patterns. The monochromatic x-ray beam was produced using a channel-cut crystal (silicon 220) and was fixed at an energy of 29.200 keV, calibrated by scanning through the tin metal K-absorption edge. The x-ray beam size was controlled by a slit system to 150 $\times$ 150 μm and then focused to a beam size of 5 (vertical) $\times$ 5 (horizontal) μm at the FWHM by Kirkpatrick–Baez mirrors [14]. Typical CCD exposure times were 60 s.

The x-ray intensity before and after the DAC was monitored by an ion chamber and a photodiode, respectively. The photodiode reading reflects the x-ray absorption of the sample and the DAC, while the reading from the ion chamber is used for normalization.

3. High-pressure melting

Diffuse scattering from indium melt is clearly observed in the CCD image (figure 1). Our results on high-pressure melting are summarized in figure 2 and compared to the piston–

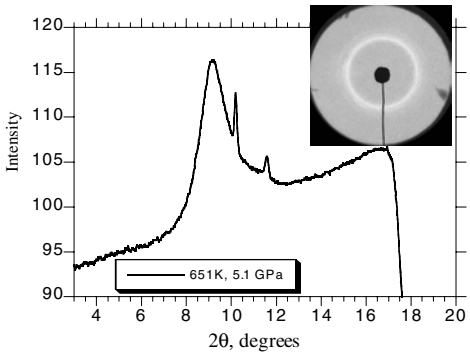

Figure 1. A typical diffuse scattering pattern of molten indium integrated from an x-ray scattering image recorded in a CCD detector (inset). A broad diffuse ring is clearly visible at around 9.5° 2θ. Two crystalline diffraction lines are from the rhenium gasket.

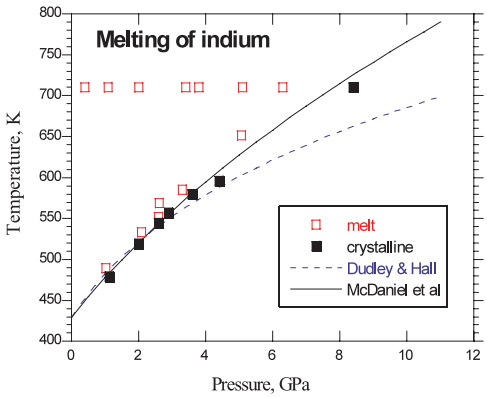

Figure 2. High-pressure melting curves for indium. The symbols show the results of this study with errors bars comparable to or less than the symbol size. An experimental path of isothermal compression at 710(3) K is also shown.

cylinder results of Dudley and Hall [15] and McDaniel *et al* [16]. Our data show slightly higher melting temperatures than those of Dudley and Hall [15]. As pointed out in a later work [17], the pressure scale in Dudley and Hall's work needs to be revised downward in accordance with the fixed points of solid–solid transitions obtained by Kennedy and La Mori [18]. After pressure correction, the melting curve of Dudley and Hall [15] is almost identical to that of McDaniel *et al* [16]. Clearly, our data support the correction [17].

4. Density of melts

A standard was introduced in the sample preparation for measuring the density of molten indium. From the known density of the standard material determined by x-ray diffraction, the thickness of the sample chamber can be obtained. One typical x-ray transmission scan is given in figure 3 with the monochromatic beam of 29.200 keV. According to the absorption law: $I = I_0 \exp(-\mu\rho l)$, where I is the transmission intensity, I_0 the normalized incident intensity, μ the mass absorption coefficient, ρ the density, and l the thickness of the sample, the thickness (l) can be obtained from

$$\text{thickness } (l) = \ln(I_{\text{NaCl}}/I_{\text{Re}})/(\mu_{\text{Re}}\rho_{\text{Re}} - \mu_{\text{NaCl}}\rho_{\text{NaCl}}). \tag{1}$$

The quantities in the right-hand side of equation (1) are either known values (μ) or measurable (ρ and I). The x-ray transmission can be directly measured as shown in figure 3; the mass absorption coefficients at 29.200 keV is obtained from a report [19] by the National Bureau of Standards; the densities of NaCl and rhenium are obtained by x-ray diffraction since these two materials were in crystalline states in the pressure–temperature range of this study. By assuming the same thickness across the sample and the standard, we obtain the density of the molten state:

$$\rho_{\text{In}} = [\ln(I_{\text{NaCl}}/I_{\text{In}}) + \mu_{\text{NaCl}}\rho_{\text{NaCl}}l]/\mu_{\text{In}}l. \tag{2}$$

It should be noted that the distance between two diamond anvils is not always the same across the culet area. Especially at pressures over 30 GPa, deformation occurs with diamond anvils [20], resulting in a variable thickness profile. In this case, a two-dimensional scan is required for obtaining a thickness profile across the whole culet area [21].

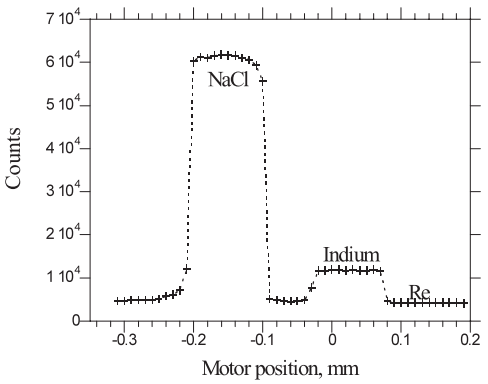

Figure 3. X-ray transmission intensities measured by a photodiode across the sample and the standard (NaCl). The monochromatic x-ray beam was at 29.200 keV. The step size for the scan was 5 μm. Small x-ray beam size is critical for a reliable measurement.

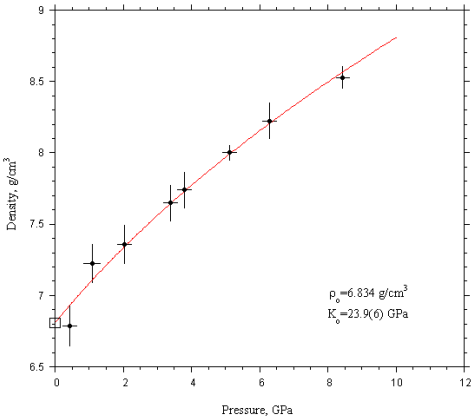

Figure 4. Densities of molten indium at 710(3) K at high pressures. The value at ambient pressure (open square) is from [22]. The curve is the fit with the second-order Birch–Murnaghan equation of state with the parameters shown in the figure.

The transmission data shown in figure 3 were measured at the condition (3.4 GPa and 448 K) where the indium was in the crystalline state. By measuring its x-ray diffraction, we obtained a density of 7.667(16) g cm^{-3} for the crystalline indium. By absorption measurement and employing equations (1) and (2), we obtained a thickness of 51.39(22) μm and a density of 7.72(11) g cm^{-3}, where the standard errors were estimated by the errors in the x-ray transmission intensities and in the molar volumes obtained by diffraction. The relative error ($\Delta\rho/\rho$) obtained by the absorption method is 1.4% compared to that (0.2%) obtained by diffraction. The density difference between the two methods is 0.053 g cm^{-3}, which is within the standard error of 0.11 g cm^{-3} given by the absorption method. We found that the main error source in the absorption method is the transmission intensities. Some irregularities can be seen from the transmission profile (figure 3). More improvement can be achieved by using a cleaner x-ray beam less than 5 μm in size and a longer collecting time to achieve better statistics. A proper choice of energy and the standard material will also help to produce an optimal intensity contrast between the material under study and the standard.

As can be seen in figure 2, we performed an isothermal compression at 710(3) K. The compression behaviour of molten indium is given in figure 4. The temperature dependence of the densities of molten indium at room pressure was measured by the sessile-drop method [22], which gives the density of indium at 710 K as 6.834 g cm^{-3}. The ambient pressure data are consistent with the extrapolation of our high-pressure results. The line in figure 4 is the fit with the Birch–Murnaghan equation of state with parameters of $K_0 = 23.9(6)$ GPa and $K' = 4$ obtained by fixing $\rho_0 = 6.834$ g cm^{-3}. From the compression data [23–25] at 300 K for crystalline indium, the Birch–Murnaghan equation-of-state parameters are $\rho_0 = 7.310$ g cm^{-3}, $K_0 = 45.7(6)$ GPa, $K' = 5.2(2)$ GPa. Clearly, the melt is more compressible than the corresponding solid.

5. Structure of melts

The observed x-ray scattering intensity $I^{obs}(Q)$ may be expressed by [26]

$$I^{obs}(Q) = PA[I^{coh}(Q) + I^{inc}(Q) + I^{mul}(Q) + I^{back}(Q)], \tag{3}$$

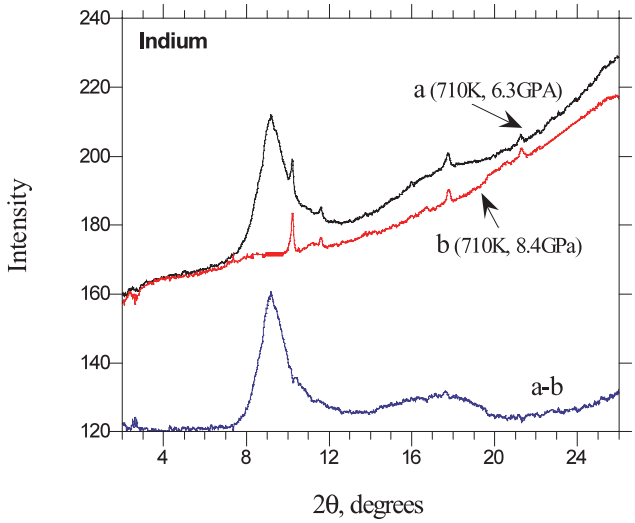

Figure 5. An illustration of obtaining the coherent scattering of molten indium. By subtracting the x-ray scattering (b) of the corresponding crystalline phase at P–T conditions close to melting, the coherent scattering from the melt can be obtained (a − b). A few crystalline peaks from the rhenium gasket exist in the original patterns, which can also be subtracted as shown.

where $Q = 4\pi \sin(\theta)/\lambda$, P is the polarization factor, A the absorption factor, and I^{coh}, I^{inc}, and I^{mul} are the coherent, incoherent, and multiple-scattering intensities, respectively. I^{back} is the background scattering intensity from surrounding materials (diamond anvils in this case). I^{mul} is relatively weak and is usually neglected in x-ray scattering [26, 27]. I^{coh} can be expressed as $f_a^2 S(Q)$, where f_a is the atomic scattering factor and $S(Q)$ the structure factor. To obtain $S(Q)$, the incoherent scattering (I^{inc}) and background scattering (I^{back}) have to be subtracted from the observed intensity.

After a few cycles of melting and solidification, crystal growth of the indium sample occurred, often resulting in the disappearance of the diffraction signals from the crystalline phase. The absence of crystalline diffraction gives an ideal reference for subtracting the incoherent and the background scattering. Figure 5 shows an example of how I^{coh} was obtained. The x-ray scattering patterns at conditions just above (pattern a) and below (pattern b) melting are shown. Pattern b from the crystalline phase includes information on I^{inc} and I^{back} in equation (3) (e.g., the Compton scattering of the diamond anvils and the sample). By subtracting pattern b from that of the molten phase (pattern a), the coherent scattering $I^{coh}(Q)$ can be obtained.

The diffraction intensity was then converted into the structure factor, $S(Q) = NI^{coh}(Q)/f_a^2(Q)$, where N is the normalization factor for $S(Q) \to 1$ at $Q \to \infty$. Figure 6 shows the structure factors measured at various pressures at a temperature of 710(3) K. From $S(Q)$, the pair distribution function, $g(r)$, is given by Fourier transformation of $Q_i(Q) = Q[S(Q) - 1]$. The density data measured in this study were used in the calculation of $g(r)$ (figure 7).

The pair distribution function $g(r)$ of molten indium shows a sharp first peak at about 3.0 Å and a broad second peak around 6.5 Å. There are some spurious ripples on both sides of the first peak, and the first peak is broader than those reported at 1 bar [28, 29], even that at 1.0 GPa, which may result from the limited range of Q over which the $S(Q)$ were measured and from errors in the $S(Q)$ themselves. Therefore, it is important to have large Q-coverage

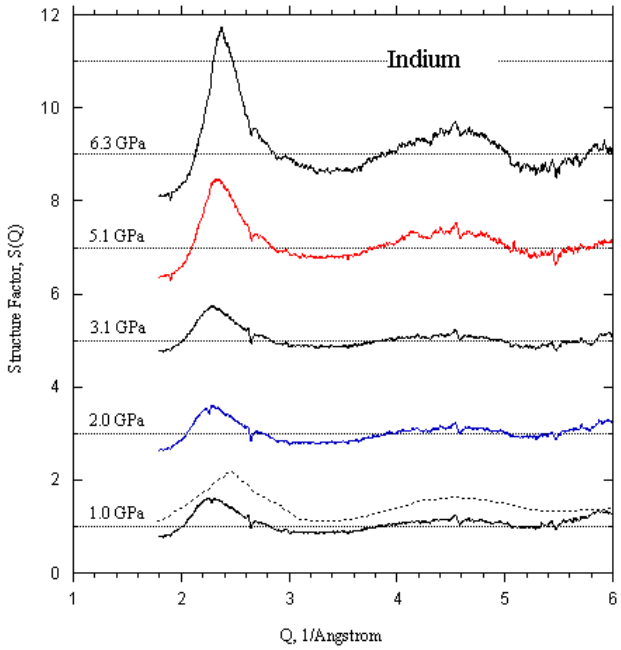

Figure 6. Structure factors of molten indium as a function of pressure at a temperature of 710(3) K. It can be seen that the intensity of the first peak increases with pressure increasing. The dotted line shows the data at 1 bar and 773 K [29] for comparison.

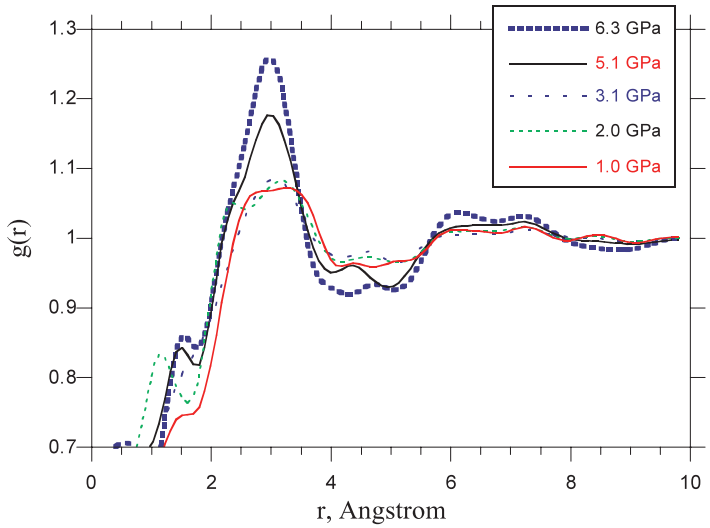

Figure 7. The pair distribution function $g(r)$ of molten indium at 710(3) K.

for studying the structure of amorphous materials in a DAC. With increasing pressure, the first peak of $g(r)$ becomes sharper and more intense, indicating that the atoms are more localized around the nearest neighbour. This effect is also noticeable in $S(Q)$ (figure 6) where the intensity of the first peak at around Q of 2.3 Å^{-1} increases with pressure. With the concept of the coordination number (CN) at the nearest neighbour, this phenomenon can be described

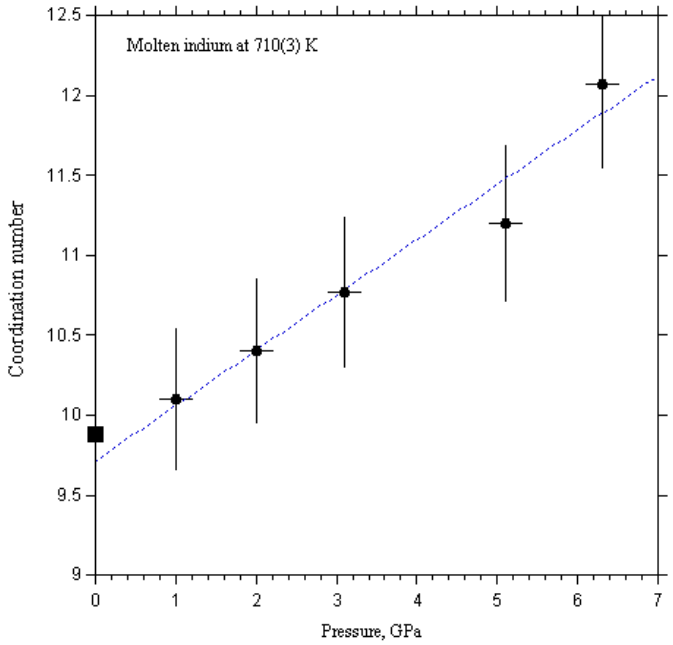

Figure 8. The coordination number of the nearest neighbours of molten indium as a function of pressure at 710(3) K. The error bars are at the ±5% level, a value estimated from errors in $g(r)$. Uncertainties arising from the errors in density are less than 2%. Uncertainties arising from the choice of the limits on both sides of the first peak in $g(r)$ could be as large as 30%. Data at 1 bar (■) are from [29].

in a quantitative way. The CN was calculated by the integration of the first peak in the radial distribution function, RDF $= 4\pi r^2 g(r)$, from zero to the first minimum after the first peak (r_{min} of 4.0 Å). The result (figure 8) shows that the CN increases with pressure almost linearly within experimental errors.

Acknowledgments

This work was supported by NSF-EAR 0001149. The GSECARS sector is supported by the NSF (Earth Science Instrumentation and Facilities Program) and the DOE (Geoscience Program).

References

[1] Datchi F, Loubeyre P and LeToullec R 2000 *Phys. Rev.* B **61** 6535
[2] Shen G and Lazor P 1995 *J. Geophys. Res.* **100** 17 699
[3] Shen G, Sata N, Rivers M L and Sutton S R 2001 *Appl. Phys. Lett.* **78** 3208
[4] Tsuji K, Yaoita K, Imai M, Shimomura O and Kikegawa T 1989 *Rev. Sci. Instrum.* **60** 2425
[5] Urakawa S, Igawa N, Shimomura O and Ohno H 1999 *Am. Mineral.* **84** 341
[6] Katayama Y, Mizutani T, Utsumi W, Shimomura O and Tsuji K 2001 *Phys. Status Solidi* b **223** 401
[7] Sanloup C, Guyot F, Gillet P, Fiquet G, Hemley R J, Mezouar M and Martinez I 2000 *Europhys. Lett.* **52** 151
[8] Raty J Y, Gaspard J P, Le Bihan T, Mezouar M and Bionducci M 1999 *J. Phys.: Condens. Matter* **11** 10 243
[9] Poole P H, Grande T, Angell C A and McMillan P F 1997 *Science* **275** 322
[10] Katayama Y, Mizutani T, Utsumi W, Shimomura M, Yamakata M and Funakoshi K-i 2000 *Nature* **403** 170

[11] Mishima O and Stanley H E 1998 *Nature* **396** 329
[12] Katayama Y, Tsuji K, Shimomura O, Kikegawa T, Mezouar M, Martinez-Garcia D, Besson J M, Hausermann D and Hanfland M 1998 *J. Synchrotron Radiat.* **5** 1023
[13] Sanloup C, Guyot F, Gillet P, Fiquet G, Mezouar M and Martinez I 2000 *Geophys. Res. Lett.* **27** 811
[14] Eng P, Rivers M L, Yang B X and Schildkamp W 1995 *Proc. SPIE* **2516** 41
[15] Dudley J D and Hall H T 1960 *Phys. Rev.* **118** 1211
[16] McDaniel M L, Babb S E Jr and Scott G J 1962 *J. Chem. Phys.* **37** 822
[17] Jayaraman A, Klement W Jr, Newton R C and Kennedy G C 1963 *J. Phys. Chem. Solids* **24** 7
[18] Kennedy G C and La Mori P N 1961 *Progress in Very High Pressure Research* (New York: Wiley)
[19] Berger M J and Hubbell J H 1987 *Photon Cross Sections on a Personal Computer* (Gaithersburg, MD: National Bureau of Standards)
[20] Hemley R J, Mao H K, Shen G, Badro J, Gillet P, Hanfland M and Häusermann D 1997 *Science* **276** 1242
[21] Shen G, Sata N, Rivers M L and Sutton S R 2002 *Appl. Phys. Lett.* **81** 1411
[22] McClelland M A and Sze J S 1995 *Surf. Sci.* **330** 313
[23] Vaughan R W and Drickamer H G 1965 *J. Phys. Chem. Solids* **26** 1549
[24] Takemura K 1991 *Phys. Rev.* B **44** 545
[25] Schulte O and Holzapfel W B 1993 *Phys. Rev.* B **48** 767
[26] Cusack N E 1987 *The Physics of Structurally Disordered Matter: an Introduction* (Bristol: Institute of Physics Publishing)
[27] Waseda Y 1980 *The Structure of Non-Crystalline Materials* (New York: McGraw-Hill)
[28] Orton B R and Smith S P 1966 *Phil. Mag.* **14** 873
[29] Ocken H and Wagner C N J 1966 *Phys. Rev.* **149** 122